PCCP

PAPER

View Article Online
View Journal | View Issue

Cite this: *Phys. Chem. Chem. Phys.*, 2025, **27**, 6031

Estimating advancing and receding contact angles for pure and mixed liquids on smooth solid surfaces using the PCP-SAFT equation of state

Aliakbar Roosta, *[a] Sohrab Zendehboudi [b] and Nima Rezaei [a]

Received 22nd October 2024,
Accepted 19th February 2025

DOI: 10.1039/d4cp04054f

rsc.li/pccp

Contact angle is an important measure of wetting in systems involving liquid–solid interfaces. This study focuses on estimating advancing and receding contact angles of pure and mixed liquids on smooth solid surfaces using perturbed-chain polar statistical associating fluid theory equation of state (PCP-SAFT EoS). For the receding contact angle, we propose a model in which the surface energy of a solid covered by a liquid film is approximated by the geometrical average of the surface energies of the solid and liquid. The PCP-SAFT model is used to calculate the ratio of dispersion-to-total surface energy for diverse pure and mixed liquids. The results are validated against 104 experimental data point contact angles, showing an average absolute relative deviation (AARD) of 7.4% for the advancing angle and 10.6% for the receding angle. The contact angle model uses an α-parameter, acting as a weighting factor for the solid and liquid effects on the work of adhesion. The model uses 0.75 and 0.5 for the advancing and receding contact angles, respectively. To assess the reliability of this α-parameter, we also optimized it using experimental data of contact angle. The optimized parameter was found to be 0.74 for advancing and 0.48 for receding contact angle, and the AARD values slightly reduced to 7.2% and 10.5%, respectively. The value of optimized model parameter are similar to those obtained based on the model assumptions, showing that the film surface energy is correctly represented by the geometrical average both in advancing and receding processes. The contact angle model combined with the PCP-SAFT framework also allowed to accurately predict the advancing and receding contact angles of binary liquid mixtures.

1 Introduction

The wettability of liquid–solid interfaces significantly influences the properties and behavior of materials.[1] A common way to quantify wetting is by observing the contact angle of liquid droplets on solid surfaces.[2] Advancing and receding contact angles are crucial variables in surface science and provide insights into the wetting behavior of liquids, which is pivotal in various industrial and scientific applications such as pore condensation,[3] immersion lithography,[4] fiber coatings,[5] drag reduction,[6] oil production,[7] oil/water separation,[8] agricultural pesticide sprays,[9] desalination,[10] and inkjet printing.[11]

The measurement of advancing and receding contact angles can be performed using several experimental techniques, such as sessile drop, titling plate, Wilhelmy plate, capillary rise, and centrifugation.[12] A common method involves the sessile drop technique, where a liquid droplet is deposited on a solid surface, and the contact angles are measured as the droplet volume is increased or decreased.[13] In the tilting plate method, a droplet is placed on a surface that is gradually tilted until the droplet begins to move, from which the advancing and receding angles are measured.[14] The Wilhelmy plate method involves dipping and withdrawing of a thin plate from a liquid to measure these angles by analyzing force–distance curves.[15] The capillary rise method measures contact angles by observing the behavior of a liquid in a thin capillary tube placed on a surface. For the advancing and receding contact angles, the liquid rise and fall are measured in the tube, respectively.[16] The centrifugal method involves spinning a liquid droplet on a surface. The advancing contact angle is determined by measuring the angle at the front edge of the droplet, and the receding contact angle is measured at the rear edge.[14]

While these experimental measurements are invaluable, they are time-consuming, laborious, and sensitive to surface heterogeneity and contamination.[17] Therefore, theoretical models and correlations are developed based on hydrodynamic molecular-kinetics to estimate the advancing and receding contact angles, offering a complementary approach to experimental techniques.[18] There are two main approaches to explain the contact angle hysteresis: the dynamic model describes the

[a] *Department of Separation Science, School of Engineering Science, LUT University, Lappeenranta, Finland. E-mail: aliakbar.roosta@lut.fi*
[b] *Department of Process Engineering, Memorial University, St. John's, NL, Canada*

contact angle behavior have not the contact line motion, and the other model describes the static contact angle hysteresis.[18] The dynamic models are of three types: (1) hydrodynamic models, which assume that viscous dissipation within the liquid phase is the dominant factor influencing the contact angle dynamics, including friction in the liquid film;[19,20] (2) molecular-kinetic models, which focus on the adsorption and desorption processes of molecules at the liquid–substrate interface, explaining how these molecular interactions impact the contact angle by considering the rate at which molecules attach to and detach from the surface;[21] and (3) hybrid hydrodynamic-molecular kinetic models consider both wetting line friction and viscous dissipation contributions to the dynamic contact angle.[22] The static models for advancing and receding contact angles focus on the liquid–solid interfaces under equilibrium conditions and are typically based on Young's equation.[18] Previous studies offer diverse perspectives on the static modeling of advancing and receding contact angles. Joanny and de Gennes[23] focused on the impact of surface heterogeneity on contact angle hysteresis, attributing it to defects on the solid surface. Marmur and Krasovitski[24] introduced line tension as a factor influencing the contact angle hysteresis behavior, particularly on curved surfaces. Tadmor[25] extended this concept by relating line energy to hysteresis and contact angle values. In contrast, Chibowski[26] challenged the conventional view of hysteresis as solely resulting from the surface roughness or heterogeneity. By examining liquid film formation behind the receding contact line, they proposed a new approach to estimating the solid surface free energy based on contact angle hysteresis. However, there is still no definitive consensus or complete understanding of the hysteresis phenomenon on smooth homogeneous surfaces.[27]

In our previous work,[28] we proposed a novel approach to successfully estimate the equilibrium contact angle of pure and mixed liquids on smooth solid surfaces using the perturbed chain polar statistical associating fluid theory (PCP-SAFT) equation of state and with a good acuracy. This paper presents a follow-up study and provides new correlations based on thermodynamic modelling to estimate the receding contact angle of pure and mixed liquids on smooth solid surfaces using the PCP-SAFT model. In the current study, we use a similar methodology to estimate the advancing contact angle. Commonly in literature, the receding contact angle models relate it to the advancing and equilibrium contact angle values, making its accuracy dependent on the latter estimates. The strength of our model is that the advancing and receding contact angles are estimated independently. By decoupling the advancing, receding, and equilibrium contact angle models, the uncertainty propagation from prior models is eliminated. Also, our model allows for more precise predictions across a broader range of liquid types (non-polar, polar, and associating) and solid surfaces with varying surface energies.

Our paper is structured as follows: after the introduction section, Section 2 provides background on estimating advancing and receding contact angles. Section 3 details the proposed methodology for calculating these contact angles based on the extended Young's equation.[29] In Section 4, the conditions under which the experimental data gathered from the literature are presented. Section 5 presents the results of estimations of the advancing and receding contact angles for pure and binary mixed liquids on various solid surfaces under ambient conditions. Finally, Section 6 provides the concluding remarks.

2 Theoretical background

Contact angle hysteresis is the difference between the advancing and receding contact angles and is affected by the surface pore structure and wetting history. In successive advancing–receding contact angle measurement experiments, Chibowski[26] proposed hysteresis to be primarily caused by the presence of a residual liquid film left behind the receding contact line of a droplet. This liquid film changes the effective surface free energy of the solid when calculating the receding contact angle. Chibowski[26] applied Young's equation to calculate both advancing and receding contact angles, assuming that the only difference between them is attributed to the surface energy of the solid, as demonstrated by eqn (1):

$$\gamma_{SF} = \gamma_S + \pi \quad (1)$$

where γ_S is the surface energy of the solid that is used to calculate the advancing contact angle; γ_{SF} is the film-covered solid surface energy used to calculate the receding contact angle; and π is the residual liquid film pressure. Chibowski[26] demonstrated that contact angle hysteresis arises because of the formation of a liquid film behind the receding droplet. He was inspired by the works of Bangham and Razouk[30] and Harkins and Livingstone,[31] who suggested that at equilibrium, a liquid film must be adsorbed onto the solid surface; additionally, he used Zisman's[32] concept of a monolayer forming behind the liquid droplet due to the self-assembly of the liquid molecules on the solid surface.

By knowing the surface energy of the solid and the liquid, Chibowski[26] established a relationship between the advancing and receding contact angles, as shown in eqn (2):

$$\gamma_S = \gamma_L(\cos\theta_{rec} - \cos\theta_{adv})\frac{(1+\cos\theta_{adv})^2}{(1+\cos\theta_{rec})^2-(1+\cos\theta_{adv})^2} \quad (2)$$

where γ_L is the surface energy of the liquid, and the subscripts adv and rec denote the advancing and receding contact angles, respectively.

Good *et al.*[33–35] proposed that the free energy of adhesion is equal to the geometric mean of the free energies of cohesion for the two phases in contact. At the molecular level, the geometric mean represents the average interaction strength between the solid and liquid molecules at the interface. So, it is expected that the interfacial tension can be obtained from the geometric mean of the surface energies of the two phases. Recent studies[36,37] combined the Good's geometrical mean approximation with the molecular dynamics framework to predict key parameters such as interfacial tensions and contact angles for

various liquids and substrates. These studies support the validity of Good's assumption.

In developing eqn (2), Chibowski[26] used the following work of adhesion terms based on the Good's model assumption:[33]

$$W_{adv} = 2\Phi\sqrt{\gamma_S\gamma_L} \quad (3)$$

$$W_{rec} = 2\Phi\sqrt{\gamma_{SF}\gamma_L} \quad (4)$$

where W denotes the work of adhesion and Φ is the Good's parameter ($0.5 < \Phi < 1.15$).[33] For polar or associating fluids, the work of adhesion correlation from eqn (5) is more suited.[29]

$$W_{adv} = 2\sqrt{\gamma_S^d\gamma_L^d} + 2\sqrt{\gamma_S^{nd}\gamma_L^{nd}} \quad (5)$$

where the superscripts d and nd refer to the dispersion interactions and non-dispersion (polar or associating) interactions, respectively. In our previous work,[28] it was demonstrated that using eqn (5) with extended Young's equation (Owens–Wendt–Kaelble equation (eqn (6)))[29] can lead to accurate estimations of the equilibrium contact angle.

$$\cos(\theta_{eq}) = 2\frac{\sqrt{\gamma_L^d\gamma_S^d} + \sqrt{\gamma_L^{nd}\gamma_S^{nd}}}{\gamma_L} - 1 \quad (6)$$

where the subscript eq denotes the equilibrium contact angle. In our previous work,[28] we introduced a novel methodology using the PCP-SAFT equation of state (EoS) to predict the ratio $\frac{\gamma_L^d}{\gamma_L}$ by calculating the dispersion and non-dispersion (polar or hydrogen bonding) contributions to the Helmholtz free energy. We used the Owens–Wendt–Kaelble[29] equation shown in eqn (6), as an extention of Young's equation, to estimate the equilibrium contact angle for various pure and mixed liquids on diverse solid surfaces. This includes 24 solids and 15 liquids, encompassing polar, non-polar, and associating liquids. However, our previous work[28] is limited to cases where the surface energy of the liquid exceeds that of the solid.

Inspired by Chibowski[26] and following our previous work,[28] a model is proposed to estimate the advancing and receding contact angles.

3 Methodology

Following Chibowski's hypothesis,[26] we also include in the receding contact angle model the effect of the residual liquid film on the solid surface energy. This liquid film, as suggested by Chibowski,[26] alters the effective surface free energy of the solid. Building upon Good's work[33] and using interfacial tension as the geometric mean of the surface energies, we propose that the surface energy of the film-covered solid (γ_{SF}) can be approximated as the geometric mean of the surface energies of the solid and the liquid, which is implemented for both the dispersion and non-dispersion contributions to the surface energy as shown by eqn (7) and (8):

$$\gamma_{SF}^d = \sqrt{\gamma_L^d\gamma_S^d} \quad (7)$$

$$\gamma_{SF}^{nd} = \sqrt{\gamma_L^{nd}\gamma_S^{nd}} \quad (8)$$

The geometric mean provides a balanced approximation that reflects the combined effects of the solid and liquid surface energies. A recent study[38] shows that the physical properties of a thin film arise from both the solid and liquid phases, which is a further validation of our assumption.

While our approach is consistent with the previous studies, including Chibowski's work,[26] further justification and validation of this assumption will be provided by comparing the results with experimental data of the receding contact angle.

By substituting eqn (7) and (8) into eqn (6), a new model is developed for calculating the receding contact angle as shown in eqn (9); after mathematical manipulations, eqn (10) is obtained:

$$\cos(\theta_{rec}) = 2\frac{\sqrt{\gamma_L^d\sqrt{\gamma_L^d\gamma_S^d}} + \sqrt{\gamma_L^{nd}\sqrt{\gamma_L^{nd}\gamma_S^{nd}}}}{\gamma_L} - 1 \quad (9)$$

$$\cos(\theta_{rec}) = 2\frac{(\gamma_L^d)^{0.75}(\gamma_S^d)^{0.25} + (\gamma_L^{nd})^{0.75}(\gamma_S^{nd})^{0.25}}{\gamma_L} - 1 \quad (10)$$

By comparing eqn (6) and (10), it follows that both equations are in the following form:

$$\cos(\theta)_{adv\ or\ rec} = 2\frac{(\gamma_L^d)^{\alpha}(\gamma_S^d)^{1-\alpha} + (\gamma_L^{nd})^{\alpha}(\gamma_S^{nd})^{1-\alpha}}{\gamma_L} - 1 \quad (11)$$

where $\alpha = 0.5$ for calculating the advancing contact angle and $\alpha = 0.75$ for calculating the receding contact angle.

In the current study, we evaluate eqn (10) to estimate the receding contact angle and compare it with the receding contact angle measurements from the literature. Furthermore, given that the advancing contact angle is commonly calculated using Young's equation in the literature,[26,39–41] we employ eqn (6) to estimate the advancing contact angle and compare its results with experimental data available in the literature.

Moreover, we use the literature contact angle data to optimize the power parameter term of α in eqn (11) for calculating both the advancing and receding contact angles, aiming to develop more accurate models for estimating contact angle hysteresis. Also, this method will enable to check the validity of our assumption (eqn (7) and (8)) to obtain the dispersion and non-dispersion contributions to the liquid film surface energy as the geometric mean of the surface energies of the solid and liquid. The average absolute relative deviation (AARD) between the estimated contact angles and the literature data is minimized to determine the optimal α for calculating both the advancing and receding contact angles.

4 Data collection and sources

In this study, we have compiled 104 pairs of advancing and receding contact angle data points from various liquid–solid systems available in the literature.[41–59] These data encompass contact angle measurements under the ambient conditions for a variety of liquid–solid pair combinations, including both pure

Table 1 Total surface energy (γ_S) and dispersive surface energy (γ_S^d) for different solids under room conditions

No.	Solid component (Tag)	γ_S mN m^{-1}	γ_S^d mN m^{-1}	Ref.
1	Polytetrafluoroethylene (PTFE)	19.1	18.6	60
2	Paraffin wax (Wax)	25.4	25.4	60
3	Polychlorotrifluoroethylene (PCTFE)	27.5	23.9	61
4	Polyethylene (PE)	33.1	32.0	60
5	Polystyrene (PS)	42.0	41.4	60
6	Polycarbonate (PC)	46.0	45.0	62
7	Stainless steel-316 (SS-316)	39.0	37.0	63
8	Silicon rubber (SR)	20.9	20.8	64
9	Polypropylene (PP)	30.4	30.4	65
10	Polyvinylchloride (PVC)	41.5	39.8	61
11	Polymethyl methacrylate (PMMA)	40.2	35.8	61
12	Nylon 66 (Nylon-66)	43.2	34.1	60
13	Polyvinylidene fluoride (PVDF)	30.0	23.2	60
14	Polyethylene terephthalate (PET)	41.3	37.8	60
15	Fluorinated ethylene propylene (FEP)	16.9	14.3	66
16	Polydimethylsiloxane (PDMS)	10.6	9.2	67
17	FC-732	11.3	10.8	This work
18	Nylon-12	35.8	30.3	68
19	Polybutylene terephthalate (PBT)	46.2	44.6	69
20	Thermoplastic polyolefins (TPO)	31.8	31.3	70
21	Polyperfluoro alkoxyethylene (PFA)	17.4	17.1	42
22	Ethylene tetrafluoroethylene (ETFE)	18.0	17.5	42
23	Ethylene chlorotrifluoroethylene (ECTFE)	30.2	29.7	42
24	Perfluoroalkyl acrylate (PFAC)	9.5	9.0	71
25	Silica	64.7	48.9	72
26	Glass	62.0	26.0	73

and mixed liquids. We consider 26 different solid surfaces with a surface energy (γ_S) in the range of 9.5 mN m^{-1} to 64.7 mN m^{-1}. For these solid surfaces, the contributions from dispersion forces (γ_S^d) to the total surface energy are significant at room temperature which are listed from the literature sources, as detailed in Table 1.[42,60–73]

Furthermore, we examine 27 different liquids, including six polar, nine nonpolar, and 12 associating liquids, as listed in Table 2. The pure-component parameters of the PCP-SAFT model for these 27 liquids are gathered from the literature and are summarized in Table 2.[74–76] These parameters are used to estimate the ratio $\frac{\gamma_L^d}{\gamma_L}$ using the PCP-SAFT model, based on our previous work.[28] Additionally, liquid surface tension data are obtained from the literature.[77]

5 Results and discussion

5.1 Model validation through comparison with empirical data

The advancing and receding contact angle values obtained from our model under the room conditions are compared with experimental data, as shown in Table 3. This table includes 104 data points for various systems involving 27 pure liquids and 26 solid surfaces. As shown in Table 3, the AARD values for the advancing and receding contact angles are 7.4% and 10.6%, respectively, indicating good accuracy and model reliability for calculating the advancing contact angle (using eqn (6)), and the receding contact angle (using eqn (10)). Table 3 features solids with diverse surface energy values ranging from 9.5 to 64.7 mN m^{-1}, with perfluoroalkyl acrylate (PFAC) having the minimum and silica having the maximum values (see Table 1). The list includes polar solids such as glass for which $\frac{\gamma_L^d}{\gamma_L} = 0.42$, and non-polar solids such

Table 2 PCP-SAFT pure-component parameters collected from the literature, and $(\gamma_L^d)/\gamma_L$ values calculated by PCP-SAFT

Type of fluids	Component	CAS no.	PCP-SAFT pure component parameters								$\frac{\gamma_L^d}{\gamma_L}$ values by PCP-SAFT
			m	σ	ε/k	μ^D	k^{AB}	ε^{AB}/k	Scheme	Ref.	
Associating	Formamide	75-12-7	1.4078	3.54	550	0	0.00647	2132.38	3B	74	0.78
	Water	7732-18-5	1.5000	2.6273	180.3	0	0.0942	1804.22	4C	75	0.38
	Ethylene glycol	107-21-1	1.7108	3.7348	354.18	0	0.01627	2120.08	4C	74	0.62
	Glycerol	56-81-5	1.7740	4.1223	408.60	0	0.01123	2063.85	3B	74	0.66
	Ethanol	64-17-5	2.8866	2.9577	187.26	0	0.05533	2462.31	2B	74	0.68
	1-Propanol	71-23-8	3.6480	3.0135	213.87	0	0.03853	1980.97	2B	74	0.84
	1-Butanol	71-36-3	3.6639	3.2437	232.69	0	0.01435	2163.48	2B	74	0.87
	1-Pentanol	71-41-0	3.5903	3.4655	245.27	0	0.0139	2356.44	2B	74	0.86
	1-Hexanol	111-27-3	3.5476	3.6651	258.93	0	0.00722	2509.57	2B	74	0.86
	1-Heptanol	111-70-6	3.1954	3.9887	282.27	0	0.00298	2944.42	2B	74	0.83
	1-Octanol	111-87-5	3.431	4.0491	287.14	0	0.00239	2998.54	2B	74	0.85
	1-Nonanol	143-08-8	4.0538	3.9398	277.89	0	0.00254	2917.47	2B	74	0.87
Polar	Dimethyl sulfoxide	67-68-5	3.0243	3.2427	309.36	3.96	0	0	—	76	0.85
	Pyridine	110-86-1	2.6491	3.4665	301.81	2.19	0	0	—	74	0.97
	Nitrobenzene	98-95-3	3.2851	3.5498	313.00	4.22	0	0	—	74	0.90
	Methylene iodide	75-11-6	2.4501	3.6152	381.06	1.22	0	0	—	74	0.99
	Bromoform	75-25-2	2.4337	3.6847	351.32	0.99	0	0	—	74	0.99
	α-Bromonaphthalene	90-11-9	3.4325	3.8980	369.79	1.29	0	0	—	74	0.99
Nonpolar	*n*-Hexane	110-54-3	3.0651	3.7908	236.47	0	0	0	—	74	1.00
	n-Heptane	142-82-5	3.4941	3.7926	238.11	0	0	0	—	74	1.00
	n-Octane	111-65-9	3.8607	3.8149	241.43	0	0	0	—	74	1.00
	n-Nonane	111-84-2	4.3188	3.7972	241.29	0	0	0	—	74	1.00
	n-Decane	124-18-5	4.6267	3.8411	244.92	0	0	0	—	74	1.00
	n-Undecane	1120-21-4	4.9114	3.8203	249.51	0	0	0	—	74	1.00
	n-Dodecane	112-40-3	5.4950	3.8329	244.84	0	0	0	—	74	1.00
	n-Tetradecane	629-59-4	6.0175	3.8261	252.66	0	0	0	—	74	1.00
	n-Hexadecane	544-76-3	6.9091	3.8784	250.17	0	0	0	—	74	1.00

Table 3 Comparison of experimental and estimated advancing and receding contact angles across various solid–liquid systems

			Experiments			Model			
No.	Fluids	Solids	θ_{adv}	θ_{rec}	Ref.	θ_{adv}	ARD	θ_{rec}	ARD
1	Bromoform	PTFE	74.0	54.0	42	73.5	0.7	53.0	1.8
2	α-Bromonaphthalene		75.0	54.0	42	73.0	2.7	52.7	2.5
3	Formamide		92.3	75.1	43	84.8	8.1	63.5	15.5
4	Water		122.0	94.0	42	104.7	14.2	85.2	9.4
5	Ethylene glycol		85.4	68.7	43	84.4	1.1	66.1	3.8
6	Glycerol		105.0	79.0	42	91.9	12.5	72.3	8.5
7	Pyridine		72.0	54.0	42	64.6	10.3	46.3	14.2
8	Nitrobenzene		74.0	52.0	42	72.3	2.3	52.5	1.0
9	Methylene iodide		85.0	68.0	42	77.4	8.9	56.0	17.7
10	*n*-Octane		41.5	25.9	44	30.9	25.5	21.9	15.3
11	*n*-Nonane		43.5	27.1	44	36.7	15.6	26.1	3.8
12	*n*-Decane		44	28.5	44	40.1	8.8	28.5	0.1
13	*n*-Undecane		46	29.4	44	42.7	7.2	30.4	3.3
14	*n*-Dodecane		46	30.1	44	44.7	2.9	31.8	5.6
15	*n*-Tetradecane		47.5	30.5	44	47.8	0.5	34.0	11.6
16	*n*-Hexadecane		47.5	30.5	44	49.9	5.1	35.6	16.7
17	Water	Wax	115.0	110.0	78	106.2	7.6	105.2	4.3
18	Formamide	PCTFE	79.0	57.9	43	68.2	13.7	49.2	15.0
19	Water		99.6	73.6	43	87.3	12.4	67.3	8.5
20	Ethylene glycol		80.0	58.0	43	64.0	20.0	47.7	17.8
21	Methylene iodide		60.6	44.9	43	66.6	9.9	48.3	7.7
22	Formamide	PE	75.0	48.0	45	63.6	15.2	47.9	0.3
23	Water		95.0	65.0	45	89.9	5.4	74.3	14.3
24	Ethylene glycol		63.0	43.0	45	62.6	0.6	50.8	18.2
25	Glycerol		81.0	63.0	45	73.2	9.6	58.8	6.6
26	Formamide	PS	70.8	52.9	43	53.7	24.1	42.9	18.9
27	Water		91.0	83.0	45	86.4	5.0	75.3	9.3
28	Ethylene glycol		60.5	57.5	45	54.1	10.6	48.6	15.5
29	Glycerol		72.0	64.0	45	66.8	7.3	57.5	10.2
30	Formamide	PC	57.5	43.0	45	46.9	18.4	37.6	12.6
31	Water		83.0	68.0	45	81.8	1.5	70.8	4.1
32	Ethylene glycol		57.0	38.0	45	46.5	18.4	42.8	12.5
33	Glycerol		71.0	57.0	45	60.9	14.2	52.5	7.9
34	Formamide	SS-316	60.4	45.2	46	53.9	10.8	40.3	10.8
35	Water		80.0	59.0	46	82.5	3.2	67.7	14.8
36	Glycerol		82.0	65.0	46	64.3	21.6	51.5	20.7
37	Methylene iodide		45.0	36.0	46	43.6	3.1	31.4	12.9
38	Water	SR	109.0	90.0	47	107.4	1.5	93.0	3.3
39	Glycerol		95.0	90.0	47	93.4	1.7	78.0	13.4
40	Formamide	PP	79.5	69.0	48	73.6	7.4	65.6	4.9
41	Water		99.0	87.5	48	102.2	3.2	103.2	18.0
42	Glycerol		86.5	82.0	48	85.3	1.4	83.5	1.8
43	Dimethyl sulfoxide		61.6	47.8	48	57.2	7.2	51.8	8.3
44	Methylene iodide		65.7	52.4	48	57.1	13.2	41.0	21.8
45	Water	PVC	82.0	67.0	49	81.8	0.2	68.2	1.8
46	Water	PMMA	78.0	66.0	50	76.0	2.5	60.2	8.7
47	Ethylene glycol		54.0	38.0	51	43.9	18.6	34.6	9.1
48	Water	Nylon-66	71.0	52.0	52	67.1	5.5	51.3	1.3
49	Water	PVDF	85.5	68.9	53	80.3	6.1	60.4	12.3
50	Ethylene glycol		54.1	32.1	53	56.8	5.0	41.2	28.3
51	Methylene iodide		63.6	46.5	53	67.2	5.7	49.1	5.6
52	Formamide	PET	51.7	27.9	43	48.6	5.9	35.7	27.9
53	Water		81.0	67.0	50	77.1	4.8	62.0	7.4
54	Methylene iodide		38.1	25.7	54	41.5	8.9	30.1	17.1
55	Bromoform	FEP	75.0	58.0	42	82.2	9.5	59.9	3.2
56	α-Bromonaphthalene		76.0	64.0	42	81.9	7.8	59.6	6.9
57	Formamide		101.0	83.0	42	85.5	15.4	62.1	25.1
58	Water		119.0	98.0	42	99.4	16.5	75.7	22.7
59	Ethylene glycol		93.0	77.0	42	82.1	11.8	60.4	21.5
60	Glycerol		104.0	82.0	42	89.1	14.3	66.1	19.4
61	Pyridine		72.0	63.0	42	72.0	0.0	52.3	16.9
62	Nitrobenzene		76.0	63.0	42	76.2	0.3	55.1	12.6
63	Methylene iodide		84.0	74.0	42	85.3	1.5	62.3	15.8
64	Water	PDMS	120.0	87.5	54	110.4	8.0	84.7	3.2
65	*n*-Hexane	FC-732	52.9	40.7	41	58.2	10.1	41.6	2.3
66	*n*-Heptane		58.4	45.7	41	62.7	7.3	44.9	1.8
67	*n*-Octane		61.9	51.5	41	65.4	5.7	46.9	8.8
68	*n*-Nonane		65.4	60.1	41	68.1	4.1	48.9	18.6
69	1-Propanol		71.8	47.3	41	69.3	3.5	50.6	7.0

Table 3 (*continued*)

			Experiments			Model			
No.	Fluids	Solids	θ_{adv}	θ_{rec}	Ref.	θ_{adv}	ARD	θ_{rec}	ARD
70	1-Butanol		72.7	47.5	41	71.5	1.6	52.0	9.4
71	1-Pentanol		74.4	48.8	41	72.3	2.8	52.6	7.9
72	1-Hexanol		76.3	54.3	41	82.1	7.6	60.0	10.4
73	1-Heptanol		76.6	51.2	41	81.2	6.1	59.6	16.3
74	1-Octanol		78.8	54.6	41	75.0	4.8	54.7	0.2
75	1-Nonanol		79.0	69.0	41	75.5	4.4	54.9	20.5
76	Water	Nylon-12	77.0	56.5	55	77.4	0.5	59.8	5.8
77	Water	PBT	84.0	64.0	69	79.2	5.7	67.2	5.1
78	Water	TPO	99.0	74.0	56	94.0	5.0	79.7	7.7
79	Bromoform	PFA	74.0	57.0	42	76.7	3.6	55.4	2.8
80	α-Bromonaphthalene		76.0	61.0	42	76.2	0.2	55.0	9.8
81	Formamide		100.0	79.0	42	88.4	11.6	66.7	15.6
82	Water		121.0	90.0	42	108.0	10.7	88.9	1.2
83	Ethylene glycol		92.0	75.0	42	88.4	3.9	69.9	6.7
84	Glycerol		103.0	80.0	42	95.5	7.2	75.9	5.1
85	Pyridine		72.0	60.0	42	68.7	4.6	49.4	17.6
86	Nitrobenzene		76.0	66.0	42	76.2	0.3	55.7	15.6
87	Methylene iodide		84.0	68.0	42	79.5	5.3	57.6	15.3
88	Bromoform	ETFE	68.0	51.0	42	75.8	11.5	54.8	7.4
89	α-Bromonaphthalene		70.0	47.0	42	75.3	7.6	54.4	15.8
90	Formamide		94.0	71.0	42	86.4	8.1	64.5	9.2
91	Water		108.0	84.0	42	105.5	2.3	85.3	1.6
92	Ethylene glycol		82.0	63.0	42	85.9	4.7	66.8	6.0
93	Glycerol		96.0	75.0	42	93.1	3.0	72.8	2.9
94	Pyridine		58.0	41.0	42	67.2	15.8	48.2	17.6
95	Formamide	ECTFE	79.0	65.0	42	69.4	12.2	53.2	18.1
96	Water		99.0	78.0	42	95.4	3.6	80.6	3.3
97	Ethylene glycol		67.0	53.0	42	69.5	3.8	57.6	8.6
98	Glycerol		83.0	69.0	42	79.2	4.5	65.0	5.8
99	Methylene iodide		58.0	43.0	42	57.5	0.8	41.2	4.2
100	Water	PFAC	130	91	71	116.2	10.6	91.6	0.7
101	*n*-Dodecane		77	60	71	79.0	2.6	57.1	4.8
102	Water	Silica	42	29	58	41.5	1.2	33.7	16.0
103	Water	Glass	31.0	19.8	59	33.7	8.7	24.0	21.1
104	Formamide		23.5	15.6	59	21.7	7.6	21.2	35.8
	Overall		—	—		—	7.4	—	10.6

as paraffin wax, with $\frac{\gamma_L^d}{\gamma_L} = 1$. Table 3 encompasses various types of liquids (associating, polar, and non-polar) with a broad range of surface tension values. For instance, at 293.15 K, water has a high surface tension of 72.74 mN m^{-1}, while *n*-hexane has a low surface tension of 18.50 mN m^{-1}.[77] Furthermore, according to Table 3, the maximum relative deviations for the advancing and receding contact angles are 25.5% (for *n*-octane on PTFE) and 35.8% (for formamide on glass), respectively. Except for a few cases, the ARD% values are significantly low, demonstrating the high accuracy of our calculations, given a wide range of solid and liquid systems.

We compare our contact angle models (eqn (6) and (10)) with experimental data in Fig. 1. In Fig. 1a, the estimated advancing contact angle data are plotted against the experimental data for all 104 data points, using α = 0.50. This figure shows data scattering near the $y = x$ reference line, indicating a good match between the estimated and experimental contact angle values. Overall, we slightly underestimate the advancing contact angle, especially for higher contact angle values. This deviation arises because our model relies on the Young's equation, which calculates the equilibrium contact angle, while the advancing contact angle is inherently larger. Similarly, the receding contact angle data estimated using α = 0.75 are depicted in Fig. 1b. Again, the agreement between the estimated and experimental data points is inferred by proximity to the reference line $y = x$, highlighting the accuracy and reliability of our model in estimating both advancing and receding contact angles. The trend shown in Fig. 1b shows a lower error for the receding contact angle in systems with a lower contact angle (better wetting).

5.2 Tuning of the power term in the advancing and receding contact angle models

The contact angle model estimates (advancing and receding) depend on the magnitude of the parameter α that appears as the exponent in eqn (11). Promising results for the advancing contact angle are obtained by using α = 0.50, and for the receding contact angle by using α = 0.75. The receding contact angle values depend on a key-assumption that is formulated in eqn (7) and (8), which states that when a liquid film is present, the surface energy of the solid in contact with the liquid film is obtained as the geometric average of the solid and liquid surface energies, for both the dispersion (γ_{SF}^{d}) and non-dispersion (γ_{SF}^{nd}) contributions. Furthermore, the advancing contact angle values calculated using eqn (6) rely on the assumption that the advancing contact angle is close to the equilibrium contact angle. To check the validity of these assumptions, the parameter α is set

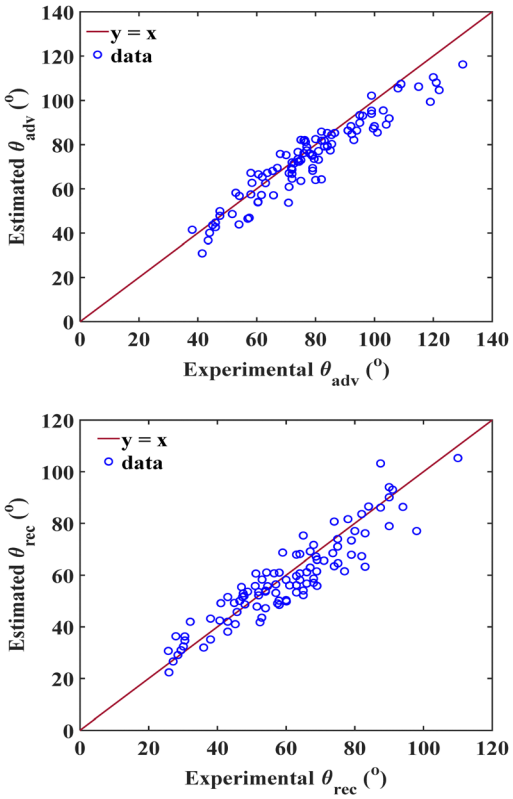

Fig. 1 A comparison between estimated and experimental contact angles, (a) advancing contact angle data using α = 0.50, and (b) receding contact angle data, using α = 0.75.

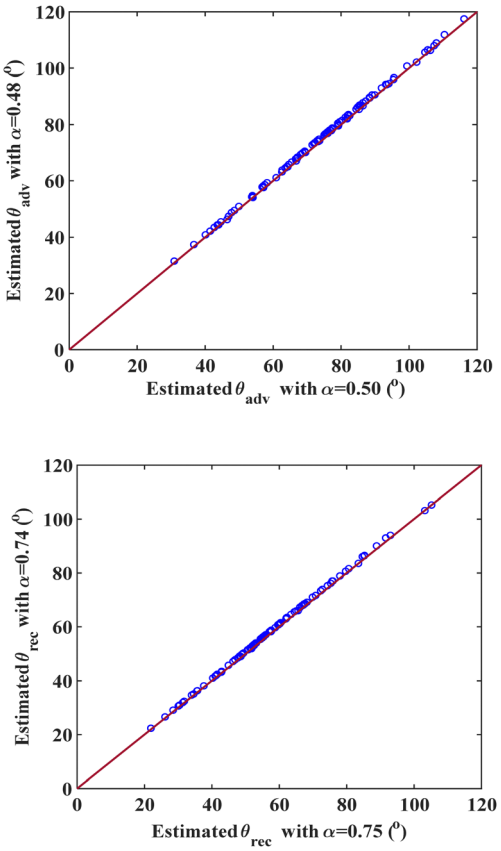

Fig. 2 A comparison between estimated contact angles using initial and optimized power terms: (a) advancing contact angle, and (b) receding contact angle. The symbols represent data, and the line is $y = x$.

to be optimized based on the experimental data. If the assumptions are not correct, then the values of α obtained from optimization will be statistically different from those obtained by implementing our model assumptions. In the optimization, the objective function is the overall AARD between the predicted and experimental contact angle values to be minimized. We employ genetic programming, as a non-linear optimization technique, focusing on minimizing AARD between the model predictions and the experimental data. This iterative process will give fine-tuned power terms for both the advancing and receding cases.

After optimization, the power term is obtained to be α = 0.48 for the advancing contact angle and 0.74 for the receding contact angle. These optimized values are remarkably close to the values 0.5 and 0.75, respectively, for advancing and receding contact angles that are obtained *a priori* based on our model assumption. Such an excellent agreement between the optimized and assumed α parameters shows the validity of our assumptions for estimating the receding contact angle (see eqn (7) and (8)) and also the applicability of eqn (6) for estimating the advancing contact angle. To assess the models' accuracy, we compare AARD% values using the initial and optimized parameter. The AARD values for the initial power terms are 7.4% and 10.6% for the advancing and receding contact angles, respectively, while the optimized power terms of 0.48 and 0.74 result in slightly lower AARD values of 7.2% and 10.5%, respectively.

The power term (α) in eqn (11) acts as a weighting factor that applies the relative influences of the solid and liquid surface energies on contact angle. For the advancing contact angle α = 0.5; so, the solid and liquid surface energies have equal weights, consistent with Young's equation. A higher α value for the receding contact angle (α = 0.75) suggests that the influence of the liquid surface energy is more dominant compared to the solid's surface energy. When the liquid recedes, the drop contacts the solid in the receding tail through a thin liquid film, where its surface energy is approximated as the geometric mean of the solid and liquid surface energies.

Fig. 2 compares the advancing and receding contact angles estimated with the optimized α values against those estimated contact angles with initial α values. As illustrated in Fig. 2, the data closely follow the $y = x$ line for the entire dataset for both advancing and receding contact angles. This suggests that using the original or optimized values of α for calculating advancing and receding contact angles yields no significant difference. To ensure this, we calculate and compare some statistical analysis parameters obtained from both the initial and optimized values of α.

The statistical analysis of the advancing and receding contact angle results with α values from optimization and that obtained *a priori* is summarized in Table 4, showing statistical parameters such as the coefficient of determination (R^2), root

Table 4 Statistical error parameters of present models to estimate θ_{adv} and θ_{rec}

		ARD (%)			AD (°)				
	α	Average (AARD%)	Min	Max	Average	Min	Max	RMSE (°)	R^2
θ_{adv}	0.50[a]	7.4	0.0	7.3	0.88	0.0	19.6	7.3	0.88
	0.48[b]	7.2	0.1	6.9	0.89	0.1	18.3	6.9	0.89
θ_{rec}	0.75[a]	10.6	0.1	7.5	0.83	0.1	22.3	7.5	0.83
	0.74[b]	10.5	0.1	7.2	0.85	0.0	21.0	7.2	0.85

[a] Used in model. [b] Optimized.

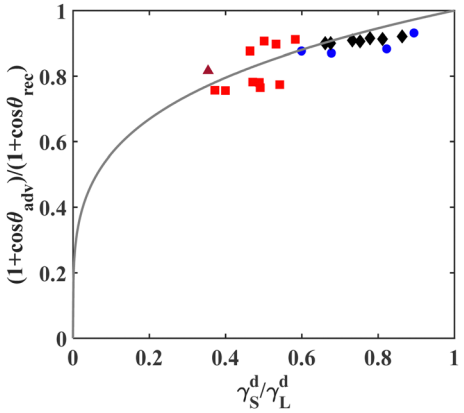

Fig. 3 Comparison of simplified contact angle relations with experimental data for non-polar substances. Line: model (eqn (14)), (●) data from ref. 48, (■) data from ref. 41, (▲) data from ref. 71, (♦) data from ref. 42.

mean square error (RMSE), average absolute relative deviation (AARD), minimum and maximum values of absolute relative deviation (min ARD and max ARD), mean absolute deviation (MAD), and minimum and maximum values of absolute deviation (min AD and max AD).

The analysis reveals that overall, the model for the advancing contact angle performs slightly better than that for the receding contact angle as it is evident in lower RMSE, AARD, and MAD values. Also, the contact angle model using the optimized power term (α) performs slightly better than that using the assumed power term values. In general, by comparing the statistical error parameters, it is evident that both the original values and optimized values of α yield nearly identical results, as the values of the statistical error parameters are similar. Hence, here on, we use α = 0.50 for the advancing contact angle and α = 0.75 for the receding contact angle in our calculations.

5.3 Simplified contact angle relationships for pure non-polar substances

When either the solid or liquid material is non-polar, the terms $\gamma_L^{nd}\gamma_S^{nd}$ will become zero. Consequently, the advancing and receding contact angles will be simplified to eqn (12) and (13):

$$\cos(\theta_{adv}) = \frac{2\gamma_L^{d^{0.5}}\gamma_S^{d^{0.5}}}{\gamma_L} - 1 \quad (12)$$

$$\cos(\theta_{rec}) = \frac{2\gamma_L^{d^{0.75}}\gamma_S^{d^{0.25}}}{\gamma_L} - 1 \quad (13)$$

The mathematical manipulation will provide a simple relationship between the advancing and receding contact angles as follows:

$$\frac{1+\cos\theta_{adv}}{1+\cos\theta_{rec}} = \left(\frac{\gamma_S^d}{\gamma_L^d}\right)^{0.25} \quad (14)$$

In eqn (14), the relationship between the advancing and receding contact angles only depends on the ratio of $\frac{\gamma_S^d}{\gamma_L^d}$. To verify this relationship for the advancing and receding contact angles when one of the substances is non-polar, eqn (14) is compared with experimental data from the literature for non-polar materials as shown in Fig. 3. The experiments include cases in which either solid or liquid is non-polar. As illustrated in Fig. 3, there is a good agreement between the experimental data and the predictions from eqn (14).

5.3.1 Non-polar liquids. When the liquid is nonpolar, two simplified relationships are obtained for advancing contact angles (eqn (15)) and receding contact angles (eqn (16)).

$$\cos\theta_{adv} = 2\left(\frac{\gamma_S^d}{\gamma_L}\right)^{0.5} - 1 \quad (15)$$

$$\cos\theta_{rec} = 2\left(\frac{\gamma_S^d}{\gamma_L}\right)^{0.25} - 1 \quad (16)$$

The simplified relationships for the case of non-polar liquids, as given by eqn (15) and (16), indicate that both the advancing and receding angles depend solely on the ratio of $\frac{\gamma_S^d}{\gamma_L}$. These correlations are plotted in Fig. 4 and are compared with experimental contact angle data from the literature. Fig. 4 demonstrates that both equations correctly predict the trends in the advancing and receding contact angles with the the ratio $\frac{\gamma_S^d}{\gamma_L}$ when the liquid is non-polar. Another observation from

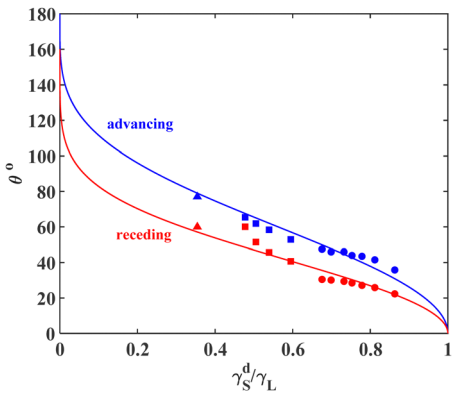

Fig. 4 Comparison of simplified contact angle models with experimental data for non-polar liquids. (▲) data from ref. 71, (■) data from ref. 41, (●) data from ref. 44.

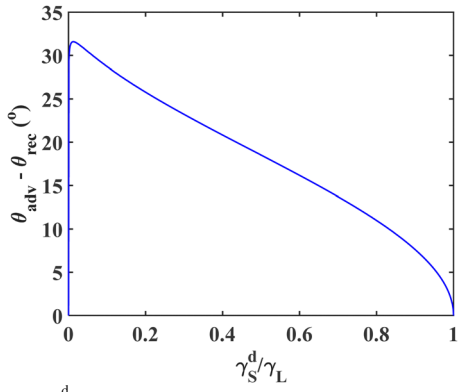

Fig. 5 Effect of $\frac{\gamma_S^d}{\gamma_L}$ on contact angle hysteresis for non-polar liquids.

Fig. 4 is that the receding and advancing contact angles approach each other when the ratio $\frac{\gamma_S^d}{\gamma_L}$ approaches either extreme values of zero or one. Based on these models, when $\frac{\gamma_S^d}{\gamma_L} = 1$, the solid surface is completely wetted by the liquid and both contact angles approach zero.

The effect of $\frac{\gamma_S^d}{\gamma_L}$ on the contact angle hysteresis ($\theta_{adv} - \theta_{rec}$) for non-polar liquids is investigated and the results are shown in Fig. 5. According to Fig. 5, decreasing the ratio of $\frac{\gamma_S^d}{\gamma_L}$ initially increases the contact angle hysteresis; the hysteresis reaches a maximum of 31.6° at $\frac{\gamma_S^d}{\gamma_L} = 0.012$, after which the it decreases sharply.

5.4 Advancing and receding contact angles of a binary liquid

We demonstrated the models to effectively predict the advancing and receding contact angles for diverse combinations of pure liquids on pure solid surfaces. In this section, we evaluate the models' capability to predict the advancing and receding contact angles for a binary liquid system, which, to the best of our knowledge, is the only available data for mixed liquids in the literature. According to our previous work,[28] the surface energy ratio $\frac{\gamma_L^d}{\gamma_L}$ for mixtures can be determined by the PCP-SAFT model by calculating the residual Helmholtz energy contributions of the liquid mixture. This ratio can be used to estimate the contact angle of mixed liquids on solid surfaces. Fig. 6 illustrates the compositional dependency of the advancing and receding contact angles for ethanol + water solutions on a PTFE surface under the ambient conditions. We evaluate the models' performance by comparing their predictions with experimental contact angle data from the literature. As it can be seen in Fig. 6, both contact angle models exhibit good accuracies in estimating the contact angles for a wide range of ethanol mole fractions in the ethanol + water mixture.

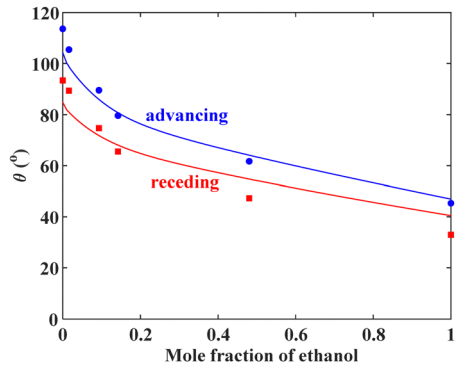

Fig. 6 Advancing and receding contact angle estimates for ethanol + water liquid mixtures on the PTFE surface *vs.* ethanol mole fraction; experimental data are obtained from ref. 57.

6 Conclusions

This study has focused on estimating the advancing and receding contact angles for pure and mixed liquids on smooth solid surfaces of diverse materials, using the PCP-SAFT equation of state. To estimate the receding contact angle, we propose a novel approach in which the surface energy of a solid containing a liquid film is approximated by the geometrical average of the pure solid and liquid surface energy values. Also, using the PCP-SAFT model, we calculate the ratio of dispersion-to-total surface energy for diverse liquids. The models are validated against 104 pairs of experimental data for advancing and receding contact angles with average absolute relative deviations (AARDs) of 7.4% and 10.6% for the advancing and receding contact angles, respectively. Such small deviations from the experimental data verify the model to be reliable and accurate in diverse liquid–solid systems tested. In the advancing and receding contact angle models, there is an α-parameter which appears in the power term. Using the model assumptions, the α-parameters for the advancing and receding contact angle models are obtained to be 0.75 and 0.50, respectively. To check the reliability of the model assumptions leading to this α-parameter value, we vary α and find its optimal values by fitting to the experimental data. After parameter optimization, the optimal α values of 0.74 and 0.48 are obtained for the advancing and receding contact angle models which are close to their corresponding values (0.75 and 0.5, respectively) obtained *a priori* in the model. As expected, the AARD% values slightly decrease (from 7.4% to 7.2% for advancing and from 10.6% to 10.5% for receding) when the α-parameter is optimized. Interestingly, these optimized α-parameter values are close to those used originally in the model, verifying the model assumptions; furthermore, the low AARD values show good model accuracy when compared to experimental data. We also simplify the contact angle correlations for the case of non-polar systems where either the liquid or solid is non-polar. The simplified models are also validated against experimental data, demonstrating their effectiveness in predicting contact angles for non-polar liquids and solids. Additionally, we extend our analysis to the contact angle of binary liquid mixtures and study the compositional dependency of advancing and receding contact angles. The models show

good accuracy in the full range of mole fractions of ethanol in ethanol/water mixtures on the PTFE surface, highlighting their applicability for liquid mixtures. Overall, the proposed advancing and receding contact angle models offer comprehensive and reliable methods for estimating the contact angles of pure and mixed liquids on smooth solid surfaces. The simplicity, versatility, and accuracy of our model make it a valuable tool for researchers and engineers working in fields related to surface science and wettability. Further research is needed, using molecular dynamics simulations and experimental studies on a wider range of systems, to deepen insights into the problem and to refine the model for more accurate predictions.

Author contributions

Aliakbar Roosta: conceptualization, data collection, programming, analysis, and writing – review and editing. Sohrab Zendehboudi: analysis and writing – review and editing. Nima Rezaei: conceptualization, supervision, and writing – review and editing.

Data availability

No new experimental data were generated for this study.

Conflicts of interest

There are no conflicts to declare.

Acknowledgements

The authors gratefully acknowledge the funding received from the Jane and Aatos Erkko Foundation (JAES) in Finland for project 210053, which enabled this research.

References

1 Y. Wang, A. Kiziltas, P. Blanchard and T. R. Walsh, ContactAngleCalculator: An Automated, Parametrized, and Flexible Code for Contact Angle Estimation in Visual Molecular Dynamics, *J. Chem. Inf. Model.*, 2022, **62**, 6302–6308.
2 T. Huhtamäki, X. Tian, J. T. Korhonen and R. H. A. Ras, Surface-wetting characterization using contact-angle measurements, *Nat. Protoc.*, 2018, **13**, 1521–1538.
3 N. K. Karna, E. Oyarzua, J. H. Walther and H. A. Zambrano, Effect of the meniscus contact angle during early regimes of spontaneous imbibition in nanochannels, *Phys. Chem. Chem. Phys.*, 2016, **18**, 31997–32001.
4 K. G. Winkels, I. R. Peters, F. Evangelista, M. Riepen, A. Daerr, L. Limat and J. H. Snoeijer, Receding contact lines: From sliding drops to immersion lithography, *Eur. Phys. J.-Spec. Top.*, 2011, **192**, 195–205.
5 D. Quéré, Fluid coating on a fiber, *Annu. Rev. Fluid Mech.*, 1999, **31**, 347–384.
6 L. Hauer, A. Naga, R. G. M. Badr, J. T. Pham, W. S. Y. Wong and D. Vollmer, Wetting on silicone surfaces, *Soft Matter*, 2024, **20**, 5273–5295.
7 A. Al-Shareef, P. Neogi and B. Bai, Dynamic contact angles in oil–aqueous polymer solutions, *Phys. Chem. Chem. Phys.*, 2017, **19**, 3337–3348.
8 S. Rasouli, N. Rezaei, H. Hamedi, S. Zendehboudi and X. Duan, Superhydrophobic and superoleophilic membranes for oil-water separation application: A comprehensive review, *Mater. Des.*, 2021, **204**, 109599.
9 P. Shah and M. M. Driscoll, Drop impact dynamics of complex fluids: a review, *Soft Matter*, 2024, **20**, 4839–4858.
10 A. A. Jamali, M. I. Vohra, A. Ali, A. Nadeem, S. M. Attia, A. Hyder, A. A. Memon, F. Khan Mahar, R. B. Mahar, J. Yang and K. H. Thebo, Highly efficient mica-incorporated graphene oxide-based membranes for water purification and desalination, *Phys. Chem. Chem. Phys.*, 2024, **26**, 16369–16377.
11 Á. G. Marín, H. Gelderblom, D. Lohse and J. H. Snoeijer, Rush-hour in evaporating coffee drops, *Phys. Fluids*, 2011, **23**, 091111.
12 H.-J. Butt, J. Liu, K. Koynov, B. Straub, C. Hinduja, I. Roismann, R. Berger, X. Li, D. Vollmer, W. Steffen and M. Kappl, Contact angle hysteresis, *Curr. Opin. Colloid Interface Sci.*, 2022, **59**, 101574.
13 X. Li, S. Silge, A. Saal, G. Kircher, K. Koynov, R. Berger and H.-J. Butt, Adaptation of a Styrene–Acrylic Acid Copolymer Surface to Water, *Langmuir*, 2021, **37**, 1571–1577.
14 S. P. Evgenidis, K. Kalić, M. Kostoglou and T. D. Karapantsios, Kerberos: A three camera headed centrifugal/tilting device for studying wetting/dewetting under the influence of controlled body forces, *Colloids Surf., A*, 2017, **521**, 38–48.
15 O. N. Tretinnikov and Y. Ikada, Dynamic Wetting and Contact Angle Hysteresis of Polymer Surfaces Studied with the Modified Wilhelmy Balance Method, *Langmuir*, 1994, **10**, 1606–1614.
16 E. Schäffer and P. Wong, Contact line dynamics near the pinning threshold: A capillary rise and fall experiment, *Phys. Rev. E:Stat. Phys., Plasmas, Fluids, Relat. Interdiscip. Top.*, 2000, **61**, 5257–5277.
17 T. T. Chau, W. J. Bruckard, P. T. L. Koh and A. V. Nguyen, A review of factors that affect contact angle and implications for flotation practice, *Adv. Colloid Interface Sci.*, 2009, **150**, 106–115.
18 H. B. Eral, D. J. C. M. 't Mannetje and J. M. Oh, Contact angle hysteresis: a review of fundamentals and applications, *Colloid Polym. Sci.*, 2013, **291**, 247–260.
19 O. V. Voinov, Hydrodynamics of wetting, *Fluid Dyn.*, 1977, **11**, 714–721.
20 R. G. Cox, The dynamics of the spreading of liquids on a solid surface. Part 1. Viscous flow, *J. Fluid Mech.*, 1986, **168**, 169.
21 Y. D. Shikhmurzaev, Moving contact lines and dynamic contact angles: a 'litmus test' for mathematical models, accomplishments and new challenges, *Eur. Phys. J.-Spec. Top.*, 2020, **229**, 1945–1977.
22 H. B. Eral, D. J. C. M. 't Mannetje and J. M. Oh, Contact angle hysteresis: a review of fundamentals and applications, *Colloid Polym. Sci.*, 2013, **291**, 247–260.

23 J. F. Joanny and P. G. de Gennes, A model for contact angle hysteresis, *J. Chem. Phys.*, 1984, **81**, 552–562.
24 A. Marmur and B. Krasovitski, Line Tension on Curved Surfaces: Liquid Drops on Solid Micro- and Nanospheres, *Langmuir*, 2002, **18**, 8919–8923.
25 R. Tadmor, Line Energy and the Relation between Advancing, Receding, and Young Contact Angles, *Langmuir*, 2004, **20**, 7659–7664.
26 E. Chibowski, Surface free energy of a solid from contact angle hysteresis, *Adv. Colloid Interface Sci.*, 2003, **103**, 149–172.
27 D. Behnoudfar, M. I. Dragila, D. Meisenheimer and D. Wildenschild, Contact angle hysteresis: A new paradigm?, *Adv. Water Resour.*, 2022, **161**, 104138.
28 A. Roosta, S. Zendehboudi and N. Rezaei, Estimating contact angle of pure and mixed liquids on smooth solid surfaces using dispersive-to-attractive surface energy ratio from PCP-SAFT model, *Chem. Eng. Sci.*, 2024, **300**, 120607.
29 D. Y. Kwok and A. W. Neumann, Contact angle measurement and contact angle interpretation, *Adv. Colloid Interface Sci.*, 1999, **81**, 167–249.
30 D. H. Bangham and R. I. Razouk, Adsorption and the wettability of solid surfaces, *Trans. Faraday Soc.*, 1937, **33**, 1459.
31 W. D. Harkins and H. K. Livingston, Energy Relations of the Surfaces of Solids II. Spreading Pressure as Related to the Work of Adhesion Between a Solid and a Liquid, *J. Chem. Phys.*, 1942, **10**, 342–356.
32 W. A. Zisman, Influence of constitution on adhesion, *Ind. Eng. Chem.*, 1963, **55**, 18–38.
33 L. A. Girifalco and R. J. Good, A Theory for the Estimation of Surface and Interfacial Energies. I. Derivation and Application to Interfacial Tension, *J. Phys. Chem.*, 1957, **61**, 904–909.
34 R. J. Good, Contact angle, wetting, and adhesion: a critical review, *J. Adhes. Sci. Technol.*, 1992, **6**, 1269–1302.
35 R. J. Good, Equilibrium Film Pressure on a Flat, Low-Energy Solid, *Adsorption at Interfaces*, 1975, pp. 28–47.
36 A. P. Sgouros, G. G. Vogiatzis, G. Kritikos, A. Boziki, A. Nikolakopoulou, D. Liveris and D. N. Theodorou, Molecular Simulations of Free and Graphite Capped Polyethylene Films: Estimation of the Interfacial Free Energies, *Macromolecules*, 2017, **50**, 8827–8844.
37 A. Jarray, H. Wijshoff, J. A. Luiken and W. K. den Otter, Systematic approach for wettability prediction using molecular dynamics simulations, *Soft Matter*, 2020, **16**, 4299–4310.
38 K. Huang and R.-H. Yoon, Surface Forces in the Thin Liquid Films (TLFs) of Water Confined between *n*-Alkane Drops and Hydrophobic Gold Surfaces, *Langmuir*, 2019, **35**, 15681–15691.
39 C. J. van Oss, R. F. Giese and W. Wu, On the Degree to which the Contact Angle is Affected by the Adsorption onto a Solid Surface of Vapor Molecules Originating from the Liquid Drop, *J. Dispersion Sci. Technol.*, 1998, **19**, 1221–1236.
40 C. N. C. Lam, N. Kim, D. Hui, D. Y. Kwok, M. L. Hair and A. W. Neumann, The effect of liquid properties to contact angle hysteresis, *Colloids Surf., A*, 2001, **189**, 265–278.
41 C. N. C. Lam, R. Wu, D. Li, M. L. Hair and A. W. Neumann, Study of the advancing and receding contact angles: liquid sorption as a cause of contact angle hysteresis, *Adv. Colloid Interface Sci.*, 2002, **96**, 169–191.
42 S. Lee, J.-S. Park and T. R. Lee, The Wettability of Fluoropolymer Surfaces: Influence of Surface Dipoles, *Langmuir*, 2008, **24**, 4817–4826.
43 C. W. Extrand and Y. Kumagai, An Experimental Study of Contact Angle Hysteresis, *J. Colloid Interface Sci.*, 1997, **191**, 378–383.
44 M. E. Diaz, J. Fuentes, R. L. Cerro and M. D. Savage, Hysteresis during contact angles measurement, *J. Colloid Interface Sci.*, 2010, **343**, 574–583.
45 F. D. Petke and B. R. Ray, Temperature dependence of contact angles of liquids on polymeric solids, *J. Colloid Interface Sci.*, 1969, **31**, 216–227.
46 K. Terpiłowski, L. Hołysz, D. Rymuszka and R. Banach, Comparison of contact angle measurement methods of liquids on metal alloys, *Ann. Univ. Mariae Curie-Sklodowska, Sect. AA:Chem.*, 2016, **71**, 89.
47 W. G. Pitt, B. R. Young and S. L. Copper, Measurement of advancing and receding contact angles inside polymer tubing, *Colloids Surf.*, 1987, **27**, 345–355.
48 E. Chibowski and K. Terpilowski, Surface free energy of polypropylene and polycarbonate solidifying at different solid surfaces, *Appl. Surf. Sci.*, 2009, **256**, 1573–1581.
49 K. M. McGinty and W. J. Brittain, Hydrophilic surface modification of poly(vinyl chloride) film and tubing using physisorbed free radical grafting technique, *Polymer*, 2008, **49**, 4350–4357.
50 H. Y. Erbil, G. McHale, S. M. Rowan and M. I. Newton, Determination of the Receding Contact Angle of Sessile Drops on Polymer Surfaces by Evaporation, *Langmuir*, 1999, **15**, 7378–7385.
51 B. A. Johnson, J. Kreuter and G. Zografi, Effects of surfactants and polymers on advancing and receding contact angles, *Colloids Surf.*, 1986, **17**, 325–342.
52 S. L. Schellbach, S. N. Monteiro and J. W. Drelich, A novel method for contact angle measurements on natural fibers, *Mater. Lett.*, 2016, **164**, 599–604.
53 C. A. Fuentes, L. Q. N. Tran, M. Van Hellemont, V. Janssens, C. Dupont-Gillain, A. W. Van Vuure and I. Verpoest, Effect of physical adhesion on mechanical behaviour of bamboo fibre reinforced thermoplastic composites, *Colloids Surf., A*, 2013, **418**, 7–15.
54 W. S. Y. Wong, L. Hauer, A. Naga, A. Kaltbeitzel, P. Baumli, R. Berger, M. D'Acunzi, D. Vollmer and H.-J. Butt, Adaptive Wetting of Polydimethylsiloxane, *Langmuir*, 2020, **36**, 7236–7245.
55 C. W. Extrand, Water Contact Angles and Hysteresis of Polyamide Surfaces, *J. Colloid Interface Sci.*, 2002, **248**, 136–142.
56 A. Nihlstrand, T. Hjertberg and I. K. Johansson, in *First International Congress on Adhesion Science and Technology*, ed. W. J. van Ooij and H. R. Anderson, CRC Press, 1998, pp. 287–307.

57 Y. Yonemoto and T. Kunugi, Experimental and theoretical investigation of contact-angle variation for water–ethanol mixture droplets on a low-surface-energy solid, *Int. J. Heat Mass Transfer*, 2016, **96**, 614–626.
58 E. F. Ethington, Interfacial contact angle measurements of water, mercury, and 20 organic liquids on quartz, calcite, biotite, and Ca-montmorillonite substrates, USGS-OFR-90-409, 1990.
59 M. P. Chodkowski, Significance of the receding contact angle in the determination of surface free energy, *Ann. Univ. Mariae Curie-Sklodowska, Sect. AA:Chem.*, 2019, **73**, 61.
60 D. K. Owens and R. C. Wendt, Estimation of the surface free energy of polymers, *J. Appl. Polym. Sci.*, 1969, **13**, 1741–1747.
61 S. Wu, Calculation of interfacial tension in polymer systems, *J. Polym. Sci., Part C: Polym. Symp.*, 1971, **34**, 19–30.
62 *Coatings Of Polymers And Plastics*, ed. R. A. Ryntz and P. V. Yaneff, CRC Press, Boca Raton, 1st edn, 2003.
63 D. F. Williams, E. J. C. Kellar, D. A. Jesson and J. F. Watts, Surface analysis of 316 stainless steel treated with cold atmospheric plasma, *Appl. Surf. Sci.*, 2017, **403**, 240–247.
64 N. J. Hallab, K. J. Bundy, K. O'Connor, R. L. Moses and J. J. Jacobs, Evaluation of Metallic and Polymeric Biomaterial Surface Energy and Surface Roughness Characteristics for Directed Cell Adhesion, *Tissue Eng.*, 2001, **7**, 55–71.
65 K. Grundke and A. Augsburg, On the determination of the surface energetics of porous polymer materials, *J. Adhes. Sci. Technol.*, 2000, **14**, 765–775.
66 S. Ebnesajjad, *Surface Treatment of Materials for Adhesive Bonding*, Elsevier, 2nd edn, 2014, pp. 331–341.
67 E. J. Berger, *Acid-Base Interactions: Relevance to Adhesion Science and Technology berger*, VSP, Utrecht, The Netherlands, 1991.
68 S. Wu, in *Polymer Handbook*, ed. J. Brandrup, E. H. Immergut and E. A. Grulke, John Wiley & Sons, 4th edn, 1999, pp. 521–541.
69 C. Della Volpe, C. Migliaresi and G. Mari, *Surface Modification of Polymeric Biomaterials*, Springer, US, Boston, MA, 1996, pp. 107–115.
70 E. J. Berger, *Acid-Base Interactions: Relevance to Adhesion Science and Technology*, ed. K. L. Mittal, The Netherlands, 1991, p. 217.
71 E. Milnes-Smith, C. A. Stone, C. R. Willis and S. Perkin, Surface Reconstruction of Fluoropolymers in Liquid Media, *Langmuir*, 2022, **38**, 4657–4668.
72 A. Shivamurthy, G. R. Prashanth, N. M. Renukappa, J. Sundara Rajan and S. Parameshwara, Study of surface energy of SiO_2 and TiO_2 on charge carrier mobility of rubrene organic field effect transistor, in *3rd International Conference on Theoretical and Applied Nanoscience and Nanotechnology*, 2019.
73 J. Comelles, M. Estévez, E. Martínez and J. Samitier, The role of surface energy of technical polymers in serum protein adsorption and MG-63 cells adhesion, *Nanomedicine*, 2010, **6**, 44–51.
74 T. Esper, G. Bauer, P. Rehner and J. Gross, PCP-SAFT Parameters of Pure Substances Using Large Experimental Databases, *Ind. Eng. Chem. Res.*, 2023, **62**, 15300–15310.
75 E. Tsochantaris, X. Liang and G. M. Kontogeorgis, Evaluating the Performance of the PC-SAFT and CPA Equations of State on Anomalous Properties of Water, *J. Chem. Eng. Data*, 2020, **65**, 5718–5734.
76 M. Kleiner and G. Sadowski, Modeling of Polar Systems Using PCP-SAFT: An Approach to Account for Induced-Association Interactions, *J. Phys. Chem. C*, 2007, **111**, 15544–15553.
77 *Surface Tension of Pure Liquids and Binary Liquid Mixtures*, ed. M. D. Lechner, Springer-Verlag, Berlin/Heidelberg, 1997, vol. 16.
78 B. R. Ray and F. E. Bartell, Hysteresis of contact angle of water on paraffin. Effect of surface roughness and of purity of paraffin, *J. Colloid Sci.*, 1953, **8**, 214–223.

